Research Article | Vol. 11, No. 2 / 1 February 2020 / Biomedical Optics Express 699
Biomedical Optics EXPRESS

Measurement and visualization of stimulus-evoked tissue dynamics in mouse barrel cortex using phase-sensitive optical coherence tomography

PEIJUN TANG, YUANDONG LI, ADIYA RAKYMZHAN, ZHIYING XIE, AND RUIKANG K. WANG*

Department of Bioengineering, University of Washington, 3720 15th Ave NE, Seattle, WA 98195, USA
wangrk@uw.edu

Abstract: We describe a method to measure tissue dynamics in mouse barrel cortex during functional activation via phase-sensitive optical coherence tomography (PhS-OCT). The method measures the phase changes in OCT signals, which are induced by the tissue volume change, upon which to localize the activated tissue region. Phase unwrapping, compensation and normalization are applied to increase the dynamic range of the OCT phase detection. To guide the OCT scanning, intrinsic optical signal imaging (IOSI) system equipped with a green light laser source (532 nm) is integrated with the PhS-OCT system to provide a full field time-lapsed images of the reflectance that is used to identify the transversal 2D localized tissue response in the mouse brain. The OCT results show a localized decrease in the OCT phase signal in the activated region of the mouse brain tissue. The decrease in the phase signal may be originated from the brain tissue compression caused by the vasodilatation in the activated region. The activated region revealed in the cross-sectional OCT image is consistent with that identified by the IOSI imaging, indicating the phase change in the OCT signals may associate with the changes in the corresponding hemodynamics. *In vivo* localized tissue dynamics in the barrel cortex at depth during whisker stimulation is observed and monitored in this study.

1. Introduction

Optical detection of the neural activity in brain is gaining increasing interests in the field of neuroscience in recent years, because several physiological changes associated with neuronal activity can be observed by the optical methods with high spatiotemporal resolution and without requiring the use of labeling tools and invasive procedures. Cerebral hemodynamics, in particular, attracts tremendous interests as it is spatially and temporally regulated with neural activity through neurovascular coupling. The previous studies of optical neural activity imaging mainly use the optical methods such as laser speckle contrast imaging (LSCI) [1–5], laser doppler flowmetry (LDF) [6–8], near-infrared (NIR) spectroscopy [9,10], and optical coherence tomography [11–18] to detect the vascular responses to brain such as the changes in cerebral blood flow (CBF) [1,5], cerebral blood volume (CBV) [3,4], deoxyhemoglobin concentration (HbR) and oxyhemoglobin (Hb-O2) [1,2,4]. These hemodynamic-related changes are used as the markers to reveal the neural response regions. Except for the vascular responses, neuron activity is also focused. Two-photon calcium imaging is the current standard practice to directly visualize neuron activity [19–22]. However, this imaging technique requires the injection of contrast agents and the imaging time is relatively long. Further investigation of the intrinsic optical signals (IOS) generated by the activated neurons or neural tissue has also been concerned. One of the interesting findings is that the change in neural tissue volume induced by the neuronal activation can modulate the optical properties of the tissue [23–26]. This phenomenon has been observed by several techniques such as traditional microscopy imaging [26], dark-field microscope [23,25] and organic photodetector

#381332 https://doi.org/10.1364/BOE.381332
Journal © 2020 Received 22 Oct 2019; revised 4 Dec 2019; accepted 2 Jan 2020; published 9 Jan 2020

Biomedical Optics EXPRESS

(OPD) [24]. However, these optical techniques can only provide one-dimensional (1-D) signals or two-dimensional (2-D) brain-slice images in vitro, and they do not enable depth resolution.

Optical coherence tomography (OCT) is a label-free, non-contact, 3D optical imaging technique utilizing a low coherence light source and confocal detection [27]. It detects the interference signal generated between lights backscattered from the sample volume in the focal zone of the imaging optics and a reference beam of the interferometer, upon which depth-resolved image of reflectivity can be efficiently reconstructed at both high lateral (~10 μm) and axial (~7 μm) resolution. With an optical penetration depth of ~2 mm in the turbid tissue, such as cerebral cortex, OCT becomes suitable for imaging the cortex tissue in animal models in a search for the functional related signals. The relative change in OCT's intensity signal as induced by neural responses has already been reported to detect the visually evoked cortical functions in cat brain [28,29], electrically evoked (forepaw stimulation) somatosensory changes in rat brain [30,31], light activated changes in frog [32], rabbit [33], rat [34] and human [35] retinas and the electrical stimulation of the abdominal ganglion of sea slug [36]. All these studies were focused on the changes in the OCT intensity signals and did not investigate the changes in phase signal of the neural tissue during activation, which, however, may provide higher sensitivity to the refractive index change or displacement of the neural tissue.

To detect the cortical tissue responses with higher sensitivity, phase-sensitive OCT measurement [37–39] that utilizes small variations in the optical path length (OPL) may be applied to the neural activity imaging. Depth-resolved action-potential-related optical path length changes (i.e. phase changes in the OCT signals) at sub-nanometer scale has been observed from lobster and crayfish nerve preparations [40], the squid giant axon preparation [41,42] and the Drosophila CNS [43] but all these results were demonstrated *ex vivo*. The challenge for monitoring the phase signals *in vivo* in the cerebral cortex tissue is that the dynamics range of the OCT phase measurement is relatively small. Phase of the OCT signal is uniquely defined within the principal value range that is from -pi to pi, any large motion such as bulk motion, heartbeat of the living animals that exceed the principal value range would cause the phase wrapping effect, which can distort the original phase values. Hence, to investigate the phase changes of the neural tissue *in vivo*, there is a need to correct and recover the original phase values to increase the dynamics range of the OCT phase measurement and obtain the real phase change trend of the activated neural tissue.

In this paper, we apply the phase-sensitive OCT (PhS-OCT) to perform phase measurements in the depth-resolved barrel cortex of anesthetized mouse brain during whisker stimulation. Phase tracking and compensation strategies are applied to remove phase wrapping and to recover the true phase changes. Dynamic phase change of the neural tissue during functional activation is revealed for the first time *in vivo*, which may indicate a localized change in tissue volume within the activated region of the mouse brain. To guide the OCT scanning and validate the OCT results, IOS imaging system equipped with a green light laser source (532 nm) is integrated with the PhS-OCT system to provide a correlated full field relative reflectance change image that reveals the transversal 2D localized hemodynamic response area in the mouse brain. The cross-support between the two imaging modalities will be presented to delineate both vascular and cellular dynamics arising from neural activation in a single subject using one multi-functional optical system.

2. Materials and methods

2.1. Animal preparation and whisker stimulation

To perform the phase measurement in the neural tissue upon functional activation, we conducted *in vivo* imaging in the mouse brain barrel cortex before, during and after whisker stimulation. All experimental procedures in this study were approved by the Institutional Animal Care and Use Committee (IACUC) of the University of Washington and conducted in accordance with the ARRIVE guidelines. C57BL/6 mice (Charles River Laboratories, n = 6, 3-month-old, 23–25 g)

Biomedical Optics EXPRESS

were used with ketamine (80 mg/kg) and xylazine (10 mg/kg) anesthesia through intraperitoneal injection. Physiological parameters were monitored, including adequate anesthesia depth (no hindpaw reflexes) and body temperature (36.8 ± 0.2 °C) throughout all experimental procedures. Cranial window procedures were conducted similar to that described previously by Li et al [44]. The mouse cranial window was then imaged with the multi-functional optical imaging system (see Sections 2.2 and 2.3 for IOS and OCT description, respectively) before, during and immediately after the whisker stimulation. The whole imaging time was 40 s for both OCT and LSCI. Within the first 5 s, the mouse brain was in a resting state. From 5 s to 15 s, whisker stimulation was applied to the mouse. From 15 s to 40 s, whisker stimulation was stopped, and the mouse returned to the resting state. For whisker stimulation, the whiskers of the mouse were contacted circularly by a stick-connected 2-phase stepping motor for 10 seconds. The stepping motor was operated at full-step mode and synchronized with respective optical imaging system so that the stimulation and data acquisition were synchronized. To make the stick rotate at 3 Hz, 600 pulses were sent to the motor per second.

2.2. Intrinsic optical signal imaging (IOSI)

Schematic of the multi-functional imaging system is illustrated in Fig. 1. The IOSI system contained a single-mode laser diode with a wavelength of $\lambda 1 = 532$ nm (30 mW). The laser was continuously illuminating the sample. The incidence of the laser beam was at a 30° angle from the tissue surface [45,46] to minimize specular reflection. The diffusely reflected light from the tissue was detected with a CMOS camera (Basler A 504k, 1280 × 1024 pixels) through a zoom lens, which provided an adjustable magnification. The speckle size was set to twice the size of the camera pixels [47], which maximized the contrast of the speckle patterns. This was achieved by setting a magnification of 2.5 and imaging a field of view of ~5.5 × 5.5 mm. The camera exposure time was set to 40 ms and the sampling rate was set to 15 Hz. For each data set, 600 frames were captured by the IOSI system for 40 s measurement of the mouse brain.

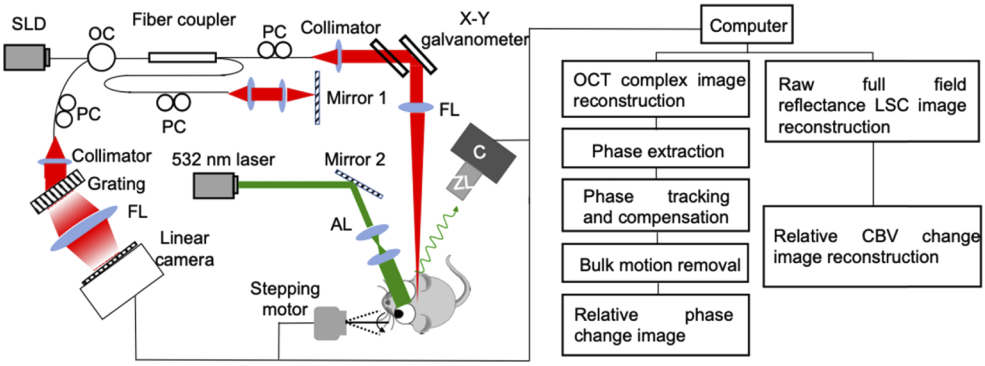

Fig. 1. Left: Schematic diagram of the multi-functional optical imaging system. SLD: superluminescent diode, OC: optical circulator, PC: polarization controller, FL: focusing lens, AL: adjusting lens, C: camera, ZL: zoom lens. Right: data processing flow chart.

After the raw reflectance images were acquired, the first 10 frames were averaged to form a baseline image. This baseline was subtracted by each of the following frames, and the resulting images were normalized to the baseline. Then, the time-lapse full field transversal 2D images representing relative changes in reflectance were obtained. The time profiles of reflectance signal change were also presented at both the activated (R1) and non-activated regions (R2). At each region, the reflectance change (-ΔR/R) signal was averaged across 6 animals.

Biomedical Optics EXPRESS

2.3. Optical coherence tomography (OCT)

A superluminescent diode (SLD) with a central wavelength of 1310 nm and a bandwidth of 110 nm was used as the light source, which yields an axial resolution of ~7 μm in air. The light from the SLD was divided into two paths through a 2 × 2 optical coupler: one for the reference arm and the other for the sample arm. In the sample arm, the light was coupled into a custom-designed optical system, containing a collimator, a pair of galvo mirrors, and an 10X objective lens with 10 μm lateral resolution [44]. The lights backscattered from the sample and reflected from the reference mirror were recombined by the 2 × 2 optical coupler, and then transmitted to a home-built spectrometer via an optical circulator for the detection of the spectral interference signal. The spectrometer had a spectral resolution of 0.141 nm, providing an imaging depth of 2.22 mm into the sample. A high speed InGaAs line scan camera (SUI, Goodrich Corp) was used in the spectrometer to capture the interferograms at a recording speed of 92,000 A-lines per second.

For the OCT scanning protocol, repeated fast B-scans were performed. Along the x-scanning direction (i.e. fast scan), 200 A-lines were captured to achieve one B-scan cross-sectional image, covering a range of ~3 mm on the sample. The duty cycle for B-scanning was ~80% per cycle, which provided a B-scan frame rate of ~300 frames per second. The system acquired 12000 B-frames to form a 40 s time course data set.

Following conventional OCT data processing [48], OCT complex images were reconstructed by the Fourier Transformation of the captured spectral interferograms by the spectrometer. Phase signal $\phi(z, t_n)$ was extracted from the OCT complex signal based on: $\phi(z, t_n) = \arctan\left(\frac{Im[I(z,t_n)]}{Re[I(z,t_n)]}\right)$, where z is the depth of the sample, t_n the time point, and $I(z, t_n)$ the OCT complex signal. $Im[]$ and $Re[]$ denote the imaginary and real parts of the OCT complex signal, respectively. To ensure that the signal we measured was from the neuronal brain tissue, we applied vascular mask and structural mask to the obtained phase signals. The structural mask was a binary image obtained by the OCT image, where the signal was set to 1 if the OCT signal strength was above twice of the noise floor, otherwise was 0. The vascular mask was also a binary image obtained by using optical microangiography (OMAG) technique [49, 50], where the signal was set to 0 if the OMAG signal strength was above twice of the noise floor, otherwise was 1. The final phase signal image was the product of the initial phase image $\phi(z, t_n)$, structural mask and vascular mask.

To recover the true phases due to dynamic change in cortical tissue during activation, the phase unwrapping methods were used. We used the phase signal in the first frame as the start point, and that in the next frame was compared with the start point. If the difference of the phase signals between adjacent frames exceeded Pi, the phase in the next frame was compensated by ±Pi. This process was repeated until the last frame was reached. In our experiment, the fast frame rate of the OCT system (300 frames/s) ensured that the phase shift during sampling interval would not exceed two cycles. This made the unwrapping method work correctly. By using this method, the unwrapped phase signals $\phi_{unwrap}(z, t_n)$ were obtained. After the phase unwrapping, all the signals were normalized to the reference signal $\phi^r_{unwrap}(t_n)$, which is stable relative to the mouse brain: $\phi_{nor}(z, t_n) = \phi_{unwrap}(z, t_n)/\phi^r_{unwrap}(t_n)$. And then, we followed the same strategy as in the IOSI processing, i.e., the first 10 frames of the phase images were averaged to form a baseline image $P_{Base} = \frac{\sum_{n=1}^{n=10} \phi_{nor}(z,t_n)}{10}$. This baseline was subtracted by each of the following frames, and the resulting image was normalized to the baseline. In doing so, the relative phase change image series were obtained as $\frac{\Delta P}{P} = \frac{\phi_{nor}(t_n) - P_{Base}}{P_{Base}}$.

3. Results

In this section, we first present the IOSI result that maps the hemodynamic changes in the mouse barrel cortex during whisker stimulation as an indication of neural activity. This resulting map provides guidance and support to the OCT imaging and phase measurements. In the phase

Biomedical Optics EXPRESS

signal analysis, to demonstrate the necessity of the recovering of the OCT's phase signals, the cross-sectional OCT phase images with and without phase tracking and compensation are presented respectively. Finally, by using the recovered phase signals, a series of cross-sectional images representing relative phase change before, during and after stimulation are presented. Tissue displacement of the activated barrel cortex at depth is measured and the localized response region at the barrel cortex, consistent with the hemodynamic change signal from IOSI reflectance maps, is visualized in the cross-sectional image.

3.1. Hemodynamic change during neural activation

Local hemodynamic change at the mouse barrel cortex during whisker stimulation was revealed by IOSI (Fig. 2). Figure 2(A) shows a schematic of the mouse cortical functional map and a photography of the cranial window delineating the region of the barrel cortex (BC). Blue circle shows the location of a 5.5 × 5.5 mm cranial window to be created, 1 mm posterior and lateral to bregma. Black dashed regions indicate the approximate locations of the BC. It can be seen that the barrel cortex region covers the right side of the cranial window in this case. A 5.5 × 5.5 mm area of cortex enclosing the entire cranial window was monitored and imaged by the IOSI system before (0~5 s), during (5~15 s) and after whisker stimulation (15~40 s). Then the relative reflectance change images were acquired and calculated by the method mentioned above. Figure 2(B) shows the relative reflectance images at the selected time points as shown. We also plotted the signal change over time at both activated region (R1) and the non-activated region (R2) as indicated in the first image in Fig. 2(B). At each region, the -ΔR/R signal was averaged and plotted in Fig. 2(C), showing as the red and black curve for R1 and R2, respectively. As indicated in the plot, the relative reflectance changes in the activated R1 began approximately 1 s after stimulation onset. As the time of the stimulus increased, the change signals in the discrete region continuously increased. After the stimulus ceased, the relative CBV change signals gradually decreased. A peak increase of changes of approximately 60% of baseline occurred 11 s after stimulus onset. On the contrary, the black curve (R2) showed no obvious responses. The high spatiotemporal resolution of the IOSI used here has accurately mapped the location of neural activity-induced hemodynamic responses and recorded the signal profile before, during, and after neural activation. The observation of the localized hemodynamic modification during functional activation is consistent with the previous studies [5]. Such mapping of the BC region is extremely useful to guide the OCT cross-sectional B-scans, and to provide support the observed local phase change in the BC upon whisker stimulation.

3.2. Phase tracking and compensation

The necessity of using phase unwrapping and normalization to reveal the dynamics of the brain tissue is illustrated by comparing the ΔP/P images at 14 s shown in Fig. 3 (during stimulation period). In the result without phase unwrapping (Fig. 3(A)), repetitive bands or striped patterns were observed caused by the phase wrapping effect, making it difficult, if not possible, to define the center of the response region. This phase wrapping effect would limit the ability to determine the true OCT phase information as shown in Fig. 3(D) where both black and red curves are wrapped within a range from -Pi to Pi. Hence, it is difficult to compare and differentiate the phase signals at R1 position (marked as white star in Fig. 3(A)) and at R2 position (yellow star) during the stimulation.

Figure 3(B) shows the ΔP/P image with phase unwrapping. The circular-like stripes are now successfully removed, and the signal contrast between the activated and non-activated regions during stimulation is revealed, where the darker color signals on the right side of the image could possibly represent the phase changes at the activated BC. In the corresponding plots in Fig. 3(E), phase change trend is recovered after the phase unwrapping. The red curve, which represents the phase signal of the pixel located at the barrel cortex (at the position as marked white star in

Biomedical Optics EXPRESS

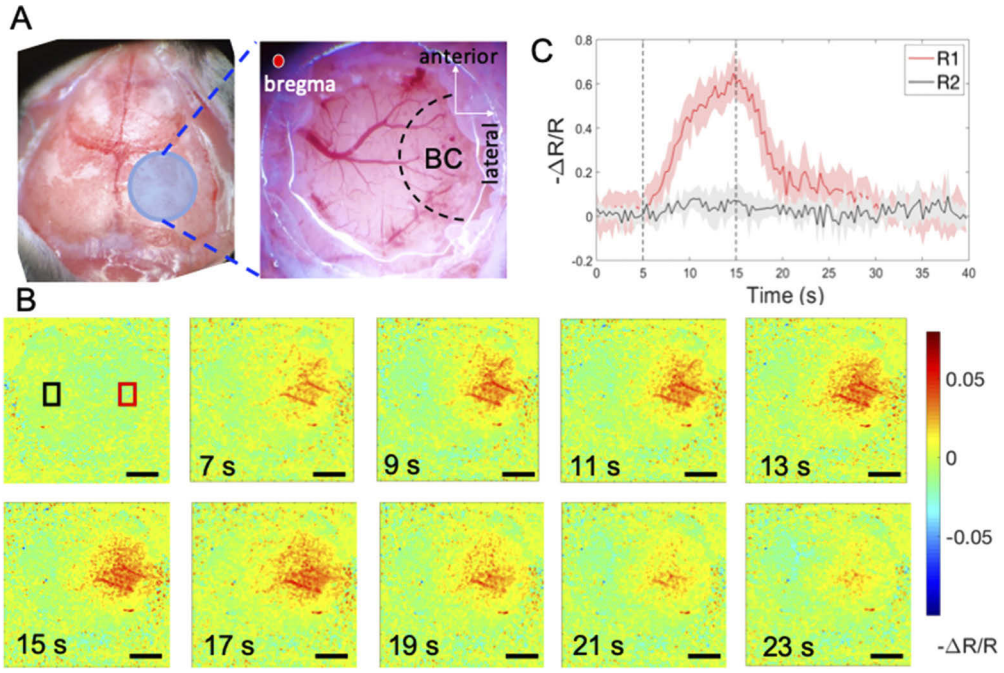

Fig. 2. Wide-field reflectance mapping of the mouse barrel cortex (BC) during whisker stimulation. A) Schematic of mouse functional cortex map and photography of the cranial window delineating the relative location of BC. B) Sequence of reflectance images indicating the relative changes in HbT contents at BC in response to 10 s of whisker stimulation; C) Time course of the relative reflectance changes averaged over a region centered on the activated area R1 (indicated by red box) and non-activated region R2 (indicated by black box) respectively. Scale bar = 1 mm.

Fig. 3(A)), decreases during the stimulation while the black curve, which is the phase signal of the pixel located at the non-response region (red star in Fig. 3(A)), remains broadly constant. However, the difference between the black and red curves begins at around 7 s, which is 2 s after the stimulation onset. It is still difficult to differentiate the difference between the black curve and red curve at the first 2 s after the stimulus onset. This is because the bulk motion, possibly caused by animal breathing or head movement during whisker stimulation, that could distort the phase signals. The blue curve in Fig. 3(E) indicates the unwrapped phase signal of the glass plate fixed on the mouse brain (the result of the cranial window preparation). The small fluctuation of the blue curve shows that there is a slow bulk motion of the mouse. When the bulk motion is large, the effective signals would be concealed. To remove the bulk motion, we used the phase signal at the surface of the glass plate as a reference for signal compensation. This selection of reference signal is reasonable because the glass plate, which is solid and fixed, should possess the same motion pattern as the mouse body. Figure 3(D) shows the ΔP/P image with phase unwrapping and compensation, where the localized response region, corresponding to the barrel cortical region, can be clearly identified. The plot in Fig. 3(F) shows the raw phase change curves corresponding to pixels in the activated and non-activated regions in Fig. 3(D) . As seen, the bulk motion is now successfully removed, leading to final true phase signal, where the measured phase at the activated region (red curve) is seen to decrease as the increase of the stimulation time duration, whereas it remains broadly stable at the non-activated region (black curve). Note that there is high frequency oscillations artifacts present in the plots, which are due to the animal heartbeats.

Biomedical Optics EXPRESS

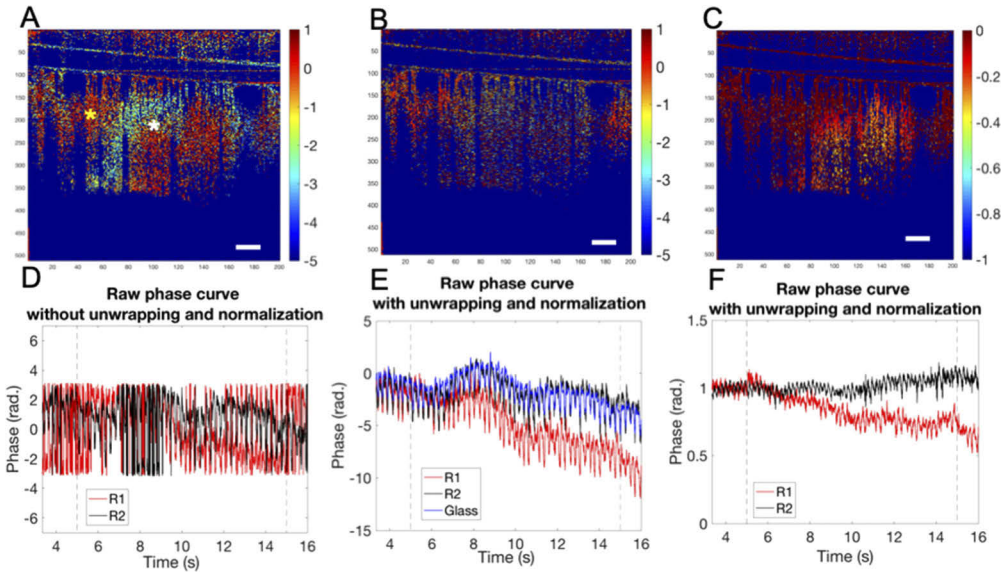

Fig. 3. Cross-sectional stimulus-induced relative phase changes (ΔP/P) mapping and curves obtained from OCT imaging. A) Relative phase change images at 12s (during whisker stimulation) without using phase unwrapping and normalization; B) Relative phase change images at 14s with phase unwrapping but without normalization; C) Relative phase change images at 14s with phase unwrapping and normalization; D), E) and F) are the corresponding time course (from 3.33 s to 15.66 s) raw phase curves for the pixels located at R1 indicated by the white star (red curve) and R2 indicated by the yellow star (black curve) in A), respectively. Scale bar = 300 μm.

3.3. Depth-resolved phase changes in neural tissue during functional activation

By applying the phase unwrapping and compensation, a sequence of cross-sectional OCT relative phase change images covering the BC before, during, and after whisker stimulation was generated and presented in Fig. 4(A). Cross-sectional OCT structure image and OMAG image were presented in Fig. 4(B) and 4(C). The whisker stimulation timeline during OCT imaging was the same as that for the IOSI, and the cross-sectional scans covered both activated and non-activated regions as indicated in the IOSI reflectance mapping, where the BC occupied relative to the right half of the OCT image frame (Fig. 4(D)). A localized ΔP/P change was observed in the BC region shortly after stimulation started at 5 s. As stimulation continued, the change in ΔP/P continued to exaggerate and expand in size. After the stimulus ceased, the ΔP/P signals gradually increased and returned to the baseline. Figures 4(F) and 4(G) plot the time course of the ΔP/P signals averaged over a region centered at the activated area and non-activated region, respectively, where the blue curves are the ΔP/P signals in R1 (indicated in the white box) and R2 (black box) corresponding to Fig. 4(A). The red curve in Fig. 4(F) is the average ΔP/P signal in the activated region while the black curve is the average ΔP/P signal in the non-activated region over 5 mice. The red curve (R1) illustrates a peak increase in phase of approximately 30% occurring 10 s after the stimulus onset. The black curve (R2) shows that there was no obvious response in R2. The shaded error bar indicates the signal variations from the data sets of the 5 mice. The averaged peak of the ΔP/P value was 0.378, with a variance of 0.06. The average delay relative to the stimulation onset time was 42.95 ms, with a variance of 15.9.

Biomedical Optics EXPRESS

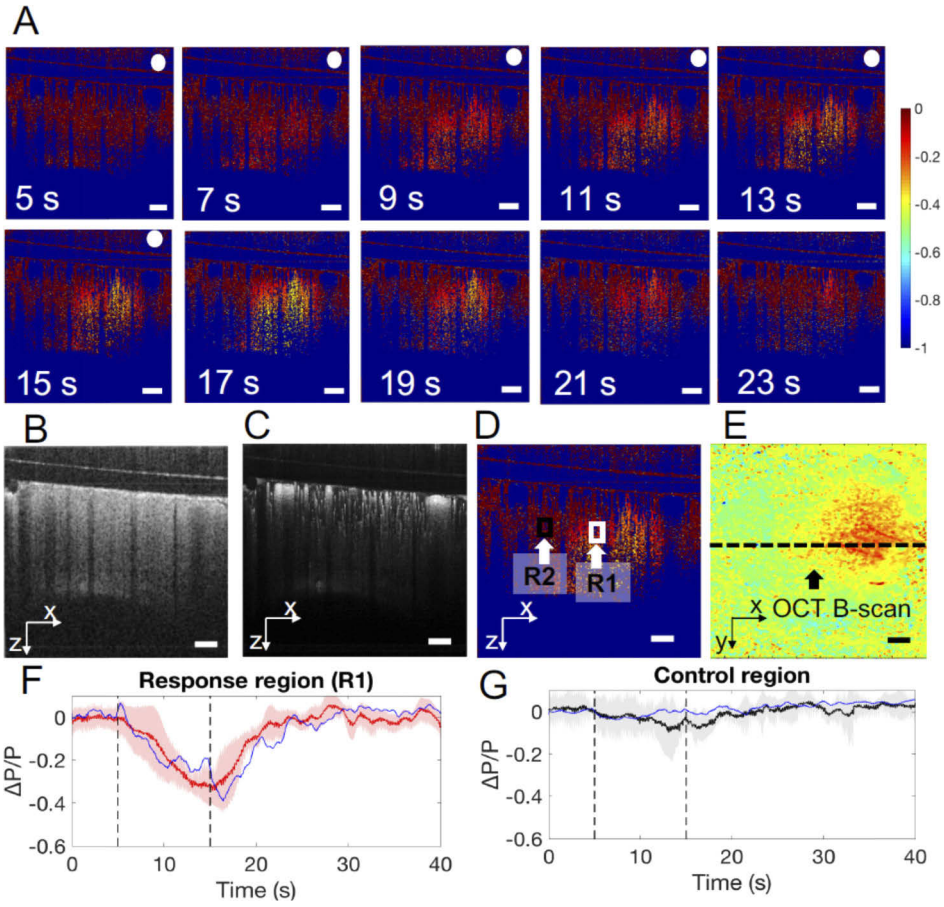

Fig. 4. Cross-sectional OCT imaging of stimulus induced changes in tissue volume in the mouse brain. A) Sequence of images showing the relative changes in tissue volume in response to 10-second whisker stimulation duration from 5s to 15s after the stimulation onset (images within the stimulation period are tagged by the white dots). Cross-sections of B) OCT structure image; C) OMAG image; D) ΔP/P image and E) IOSI image at 14 s. F) and G) Time course of ΔP/P signals averaged over a region centered on the activated area R1 (indicated in the white box) and non-activated region R2 (indicated in the black box), respectively (mean ± SEM: n = 5). Scale bar = 300 μm.

4. Discussion

The described method to properly recover the OCT phase signals has shown useful to extract the localized dynamic changes within the brain tissue upon neural simulation *in vivo*. The results demonstrated that the whisker stimulation induces a localized change in the BC, and that the spatial location and the timeline of such changes has excellent correspondence with the hemodynamics in the BC as recorded by IOSI. These observations may shed some new information in the proper understanding and interpretation of stimulus-evoked local neural activity and tissue dynamics.

It is currently not clear about the origin of phase signal change in activated cortex but can be speculated. It has been well reported in previous studies that neural activity induces arterial dilation in both pial and intracortical arterioles [51], so that blood volume can be regulated

Biomedical Optics EXPRESS

accordingly to support cerebral metabolism. The perivascular space, also known as the Virchow-Robin space, places a key factor between the neural tissue dynamics and the vasodilatory effect. The narrowing of the Virchow-Robin space from pial to deeper space occurs less than 100 μm below the cortical surface, reaching ~ 1 μm between the brain tissue and the intracortical vessels [52,53]. This means that dilations of the intracortical vessels would require a large compression of the surrounding brain tissue, causing a localized phase change (decreasing) in neural tissue during vasodilation. Due to the different Virchow-Robin space along the cortical depth, a different magnitude of such compression can be expected. Interestingly, we have observed that the magnitude of the phase change varies spatially from the pia to the deeper cortex (Fig. 4), in that the middle cortex has a higher degree of relative phase change. If this explanation holds, then whether this spatially heterogeneous response is related to the perivascular space or other mechanical properties of the brain tissue remains to be investigated. In this case, our method and observation may have a practical bearing on fMRI imaging, as it is currently still a matter of debate whether hemodynamic signal of the surface or intercortical vessels are more reliable indicators of neural activity. Therefore, it is crucial to inspect hemodynamic indicators in a depth-resolved cortex. The phase decrease may also be induced by other co-existence of mechanisms rather than the hemodynamic effect. During activation, the opening of ion channels may cause a slight change in the refractive index of the plasma which can also lead to the phase decrease [54].

This is the first time, to our knowledge, that the highly sensitive detection of OCT phase signal change was explored in the brain tissue upon neuronal stimulation *in vivo*. However, the phase accumulation effect is a potential problem in the OCT phase measurement because the phase change of the upper layer may be accumulated into the deeper layer. Further algorithm processing method needs to be explored to remove this effect. The next step in our investigation is to design a systematic study to confirm the origin of the observed phases. In this pursuit, several other imaging modalities like the adaptive OCT and two-photon imaging techniques which have higher spatial resolution could be coupled into the OCT system to image the brain activity simultaneously. By comparing the OCT phase results with the results from these imaging modalities, the origin of the observed phases may be elucidated.

5. Conclusion

We have developed a multi-functional imaging system that combines OCT with IOSI to detect the intrinsic optical markers of neural responses in mouse barrel cortex during whisker stimulation in both transversal and cross-sectional directions. IOSI was used to map and identify the regions of hemodynamic response in the activated cortex as a guidance and support to the depth-resolved OCT imaging. More importantly, a useful phase correction technique was used to overcome the OCT phase-wrapping effect and to detect localized relative phase change of the barrel cortex upon activation. The observation has presented a strong indication of the neural tissue volume change accompanied by functional brain activities. Further physiological interpretation on the observed phenomenon remains to be investigated. We expect that the optical platform and methods we developed here could be useful for observing and recording the neural responses *in vivo* and providing valuable insight of the neurovascular functions and regulations.

Funding

Facebook.

Acknowledgments

This study is supported in part by the Facebook Technologies, LLC. The funding organization had no role in the design or conduct of this research.

Biomedical Optics EXPRESS

Disclosures

None.

References

1. D. Turgut, M. G. Burnett, Y. Guoqiang, Z. Chao, F. Daisuke, A. G. Yodh, J. A. Detre, and J. H. Greenberg, "Spatiotemporal quantification of cerebral blood flow during functional activation in rat somatosensory cortex using laser-speckle flowmetry," J. Cereb. Blood Flow Metab. **24**(5), 518–525 (2004).
2. A. K. Dunn, A. Devor, A. M. Dale, and D. A. Boas, "Spatial extent of oxygen metabolism and hemodynamic changes during functional activation of the rat somatosensory cortex," NeuroImage **27**(2), 279–290 (2005).
3. L. Pengcheng, L. Qingming, L. Weihua, C. Shangbin, C. Haiying, and Z. Shaoqun, "Spatiotemporal characteristics of cerebral blood volume changes in rat somatosensory cortex evoked by sciatic nerve stimulation and obtained by optical imaging," J. Biomed. Opt. **8**(4), 629–635 (2003).
4. Y. Ma, M. A. Shaik, S. H. Kim, M. G. Kozberg, D. N. Thibodeaux, H. T. Zhao, H. Yu, and E. M. C. Hillman, "Wide-field optical mapping of neural activity and brain haemodynamics: considerations and novel approaches," Philos. Trans. R. Soc., B **371**(1705), 20150360 (2016).
5. Y. Yuan, Y. Zhao, H. Jia, M. Liu, S. Hu, Y. Li, and X. Li, "Cortical Hemodynamic Responses Under Focused Ultrasound Stimulation Using Real-Time Laser Speckle Contrast Imaging," Front. Neurosci. **12**, 269 (2018).
6. U. Dirnagl, B. Kaplan, M. Jacewicz, and W. Pulsinelli, "Continuous measurement of cerebral cortical blood flow by laser-Doppler flowmetry in a rat stroke model," J. Cereb. Blood Flow Metab. **9**(5), 589–596 (1989).
7. R. Bonner and R. Nossal, "Model for laser Doppler measurements of blood flow in tissue," Appl. Opt. **20**(12), 2097–2107 (1981).
8. M. F. Swiontkowski, "Laser Doppler Flowmetry—Development and Clinical Application," Iowa Orthop. J. **11**, 119–126 (1991).
9. F. Marco and Q. Valentina, "A brief reviw on the history of human functional near-infrared spectroscopy (fNIRS) development and fields of application," NeuroImage **63**(2), 921–935 (2012).
10. V. Quaresima and M. Ferrari, "Functional Near-Infrared Spectroscopy (fNIRS) for Assessing Cerebral Cortex Function During Human Behavior in Natural/Social Situations: A Concise Review," Organ. Res. Methods **22**(1), 46–68 (2019).
11. J. Vivek, S. Srinivasan, G. Sava, R. Iwona, W. Svetlana, James. G. Weicheng, D. A. Fujimoto, and Boas, "Depth-resolved microscopy of cortical hemodynamics with optical coherence tomography," Opt. Lett. **34**(20), 3086–3088 (2009).
12. H. Radhakrishnan and V. J. Srinivasan, "Compartment-resolved imaging of cortical functional hyperemia with OCT angiography," Biomed. Opt. Express **4**(8), 1255–1268 (2013).
13. J. Lee, J. Y. Jiang, W. Wu, F. Lesage, and D. A. Boas, "Statistical intensity variation analysis for rapid volumetric imaging of capillary network flux," Biomed. Opt. Express **5**(4), 1160–1172 (2014).
14. V. J. Srinivasan and H. Radhakrishnan, "Optical Coherence Tomography angiography reveals laminar microvascular hemodynamics in the rat somatosensory cortex during activation," NeuroImage **102**(2), 393–406 (2014).
15. P. J. Marchand, A. Bouwens, T. Bolmont, V. K. Shamaei, D. Nguyen, D. Szlag, J. Extermann, and T. Lasser, "Statistical parametric mapping of stimuli evoked changes in total blood flow velocity in the mouse cortex obtained with extended-focus optical coherence microscopy," Biomed. Opt. Express **8**(1), 1–15 (2017).
16. L. Yuandong, W. Wei, and R. K. Wang, "Capillary flow homogenization during functional activation revealed by optical coherence tomography angiography based capillary velocimetry," Sci. Rep. **8**(1), 4107 (2018).
17. P. Shin, W. Choi, J. Joo, and W.-Y. Oh, "Quantitative hemodynamic analysis of cerebral blood flow and neurovascular coupling using optical coherence tomography angiography," J. Cereb. Blood Flow Metab. **39**(10), 1983–1994 (2019).
18. W. Wei, Y. Li, Z. Xie, A. Deegan, and K. R. Wang, "Spatial and Temporal Heterogeneities of Capillary Hemodynamics and Its Functional Coupling During Neural Activation," IEEE Trans. Med. Imaging **38**(5), 1295–1303 (2019).
19. C. Stosiek, O. Garaschuk, K. Holthoff, and A. Konnerth, "Two-photon calcium imaging of neuronal networks," Proc. Natl. Acad. Sci. U. S. A. **100**(12), 7319–7324 (2003).
20. M. L. Castanares, V. Gautam, J. Drury, H. Bachor, and V. R. Daria, "Efficient multi-site two-photon functional imaging of neuronal circuits," Biomed. Opt. Express **7**(12), 5325–5334 (2016).
21. M. Li, F. Liu, H. Jiang, T. S. Lee, and S. Tang, "Long-Term Two-Photon Imaging in Awake Macaque Monkey," Neuron **93**(5), 1049–1057.e3 (2017).
22. J. Lecoq, J. Savall, D. Vučinić, B. F. Grewe, H. Kim, J. Z. Li, L. J. Kitch, and M. J. Schnitzer, "Visualizing mammalian brain area interactions by dual-axis two-photon calcium imaging," Nat. Neurosci. **17**(12), 1825–1829 (2014).
23. K. Holthoff and O. Witte, "Intrinsic optical signals in rat neocortical slices measured with near-infrared dark-field microscopy reveal changes in extracellular space," J. Neurosci. **16**(8), 2740–2749 (1996).
24. S. Rezaei-Mazinani, A. Ivanov, C. M. Proctor, P. Gkoupidenis, C. Bernard, G. G. Malliaras, and E. Ismailova, "Monitoring Intrinsic Optical Signals in Brain Tissue with Organic Photodetectors," Adv. Mater. Technol. **3**(5), 1700333 (2018).
25. O. W. Witte, H. Niermann, and K. Holthoff, "Cell swelling and ion redistribution assessed with intrinsic optical signals," An. Acad. Bras. Cienc. **73**(3), 337–350 (2001).
26. R. D. Fields, "Signaling by Neuronal Swelling," Sci. Signaling **4**(155), tr1 (2011).

Biomedical Optics EXPRESS

27. P. H. Tomlins and R. K. Wang, "Theory, developments and applications of optical coherence tomography," J. Phys. D: Appl. Phys. **38**(15), 2519–2535 (2005).
28. R. U. Maheswari, H. Takaoka, R. Homma, H. Kadono, and M. Tanifuji, "Implementation of optical coherence tomography (OCT) in visualization of functional structures of cat visual cortex," Opt. Commun. **202**(1-3), 47–54 (2002).
29. R. U. Maheswari, H. Takaoka, H. Kadono, R. Homma, and M. Tanifuji, "Novel functional imaging technique from brain surface with optical coherence tomography enabling visualization of depth resolved functional structure in vivo," J. Neurosci. Methods **124**(1), 83–92 (2003).
30. A. D. Aguirre, Y. Chen, J. G. Fujimoto, L. Ruvinskaya, A. Devor, and D. A. Boas, "Depth-resolved imaging of functional activation in the rat cerebral cortex using optical coherence tomography," Opt. Lett. **31**(23), 3459–3461 (2006).
31. C. Yu, A. D. Aguirre, R. Lana, D. Anna, D. A. Boas, and J. G. Fujimoto, "Optical coherence tomography (OCT) reveals depth-resolved dynamics during functional brain activation," J. Neurosci. Methods **178**(1), 162–173 (2009).
32. Y. Xin-Cheng, Y. Angela, P. Beth, and J. S. George, "Rapid optical coherence tomography and recording functional scattering changes from activated frog retina," Appl. Opt. **44**(11), 2019–2023 (2005).
33. K. Bizheva, R. Pflug, B. Hermann, B. Povazay, H. Sattmann, P. Qiu, E. Anger, H. Reitsamer, S. Popov, J. R. Taylor, A. Unterhuber, P. Ahnelt, and W. Drexler, "Optophysiology: depth-resolved probing of retinal physiology with functional ultrahigh-resolution optical coherence tomography," Proc. Natl. Acad. Sci. U. S. A. **103**(13), 5066–5071 (2006).
34. V. J. Srinivasan, M. Wojtkowski, J. G. Fujimoto, and J. S. Duker, "In vivo measurement of retinal physiology with high-speed ultrahigh-resolution optical coherence tomography," Opt. Lett. **31**(15), 2308–2310 (2006).
35. T. Son, M. Alam, D. Toslak, B. Wang, Y. Lu, and X. Yao, "Functional optical coherence tomography of neurovascular coupling interactions in the retina," J. Biophotonics **11**(12), e201800089 (2018).
36. L. Mariya, D. L. Marks, P. Kurt, G. Rhanor, and S. A. Boppart, "Functional optical coherence tomography for detecting neural activity through scattering changes," Opt. Lett. **28**(14), 1218–1220 (2003).
37. R. K. Wang, S. Kirkpatrick, and M. Hinds, "Phase-sensitive optical coherence elastography for mapping tissue microstrains in real time," Appl. Phys. Lett. **90**(16), 164105 (2007).
38. R. K. Wang and A. L. Nuttall, "Phase-sensitive optical coherence tomography imaging of the tissue motion within the organ of Corti at a subnanometer scale: a preliminary study," J. Biomed. Opt. **15**(5), 056005 (2010).
39. H. Spahr, C. Pfäffle, S. Burhan, L. Kutzner, F. Hilge, G. Hüttmann, and D. Hillmann, "Phase-sensitive interferometry of decorrelated speckle patterns," Sci. Rep. **9**(1), 11748 (2019).
40. T. Akkin, C. Joo, and J. F. D. Boer, "Depth-Resolved Measurement of Transient Structural Changes during Action Potential Propagation," Biophys. J. **93**(4), 1347–1353 (2007).
41. T. Akkin, D. Landowne, and A. Sivaprakasam, "Optical Coherence Tomography Phase Measurement of Transient Changes in Squid Giant Axons During Activity," J. Membr. Biol. **231**(1), 35–46 (2009).
42. Y. J. Yeh, A. J. Black, D. Landowne, and T. Akkin, "Optical coherence tomography for cross-sectional imaging of neural activity," Neurophotonics **2**(3), 035001 (2015).
43. B. H. Park, D. H. Kim, M. M. Hasan, M. R. Haque, M. S. Islam, M. E. Adams, M. Q. Tong, and S. L. Sang, "OCT intensity and phase fluctuations correlated with activity-dependent neuronal calcium dynamics in the Drosophila CNS [Invited]," Biomed. Opt. Express **8**(2), 726–735 (2017).
44. Y. Li, U. Baran, and R. K. Wang, "Application of thinned-skull cranial window to mouse cerebral blood flow imaging using optical microangiography," PLoS One **9**(11), e113658 (2014).
45. Z. Luo, Z. Yuan, Y. T. Pan, and C. W. Du, "Simultaneous imaging of cortical hemodynamics and blood oxygenation change during cerebral ischemia using dual-wavelength laser speckle contrast imaging," Opt. Lett. **34**(9), 1480–1482 (2009).
46. J. Qin, L. Shi, S. Dziennis, R. Reif, and R. K. Wang, "Fast synchronized dual-wavelength laser speckle imaging system for monitoring hemodynamic changes in a stroke mouse model," Opt. Lett. **37**(19), 4005–4007 (2012).
47. S. J. Kirkpatrick, D. D. Duncan, and E. M. Wells-Gray, "Detrimental effects of speckle-pixel size matching in laser speckle contrast imaging," Opt. Lett. **33**(24), 2886–2888 (2008).
48. R. Wang and Z. Ma, "A practical approach to eliminate autocorrelation artefacts for volume-rate spectral domain optical coherence tomography," Phys. Med. Biol. **51**(12), 3231–3239 (2006).
49. R. K. Wang, "Optical Microangiography: A Label Free 3D Imaging Technology to Visualize and Quantify Blood Circulations within Tissue Beds in vivo," IEEE J. Sel. Top. Quantum Electron. **16**(3), 545–554 (2010).
50. C. L. Chen and R. K. Wang, "Optical coherence tomography based angiography [Invited]," Biomed. Opt. Express **8**(2), 1056–1082 (2017).
51. Y.-R. Gao, S. E. Greene, and P. J. Drew, "Mechanical restriction of intracortical vessel dilation by brain tissue sculpts the hemodynamic response," NeuroImage **115**, 162–176 (2015).
52. E. T. Zhang, C. B. Inman, and R. O. Weller, "Interrelationships of the pia mater and the perivascular (Virchow-Robin) spaces in the human cerebrum," J. Anat. **170**, 111–123 (1990).
53. V. Rangroo Thrane, A. S. Thrane, B. A. Plog, M. Thiyagarajan, J. J. Iliff, R. Deane, E. A. Nagelhus, and M. Nedergaard, "Paravascular microcirculation facilitates rapid lipid transport and astrocyte signaling in the brain," Sci. Rep. **3**(1), 2582 (2013).

Biomedical Optics EXPRESS

54. B. Rappaz, P. Marquet, E. Cuche, Y. Emery, C. Depeursinge, and P. J. Magistretti, "Measurement of the integral refractive index and dynamic cell morphometry of living cells with digital holographic microscopy," Opt. Express **13**(23), 9361–9373 (2005).